

ScienceDirect



IFAC PapersOnLine 58-28 (2024) 258-263

Closed-Loop System Diagnostic based on Inverse Frequency Response Function with Application to an Electrohydraulic Actuator

Weichen Chen * Yongsoon Yoon * Neha Chaudhari ** Zongxuan Sun ***

* Department of Mechanical Engineering Oakland University, Rochester, MI 48309, USA. ** Department of Industrial & System Engineering Oakland University, Rochester, MI 48309, USA. *** Department of Mechanical Engineering University of Minnesota, Minneapolis, MN 55455, USA.

Abstract: This paper presents a closed-loop system diagnostic based on real-time estimation and monitoring of an inverse frequency response function for fault detection and isolation in an electrohydraulic actuator. Firstly, an adaptive Kalman filter is incorporated into an indirect two-stage inverse model estimation scheme to prevent covariance windup and enhance noise immunity. Secondly, rather than using estimated inverse model parameters directly, an inverse frequency response function is computed using the estimated parameters and monitored in real-time as a diagnostic residual, which is essential for the proposed diagnostic. Numerical validation with an electrohydraulic actuator demonstrates the robust fault-tracking performance, enabling robust fault detection and isolation.

Copyright © 2024 The Authors. This is an open access article under the CC BY-NC-ND license (https://creativecommons.org/licenses/by-nc-nd/4.0/)

Keywords: Fault detection & isolation; Closed-loop identification; Inverse transfer function; Adaptive Kalman filter; Electrohydraulic systems.

1. INTRODUCTION

A system diagnostic that aims to immediately detect and isolate faults of a system when they occur plays an important role in the field of industrial machinery Frank (1990); Chen and Patton (2012). Reliable fault diagnosis enables timely intervention and prevents minor faults from escalating into more serious and costly issues. It also helps optimize system performance by identifying inefficient configurations or misalignments. However, as the complexity of modern industrial machinery continues to grow, it becomes vulnerable to complicated fault mechanisms, making the design of a robust system diagnostic challenging.

An electrohydraulic actuator (EHA) is a powerful actuation device broadly used across various industries such as automotive, aerospace, marine, agriculture, mining and construction. This popularity stems from its high power density, load capacity, flexible packaging, control accuracy, and efficient maintenance Karpenko and Sepehri (2009); Boaventura et al. (2012). However, due to the presence of moving parts driven by highly pressurized working fluid, EHAs are susceptible to a range of potential faults, including sealing failure and fluid contamination with abrasive particles, air and water. These faults can adversely affect performance, energy efficiency, system bandwidth, and load capacity Eaton (1996). If the challenge of ensuring reliable diagnosis remains unsolved for contemporary industrial equipment, it could result in significant repercussions. In the most severe cases, these repercussions may include permanent

damage, substantial downtime expenses, and severe harm to operators Forbes Technology Council Post (2022).

Fault detection and isolation enable timely maintenance of equipment, which helps improve overall efficiency and production capability. Toward this end, a physics-based model is essential for understanding fault mechanism if it is available. If not available, likely due to system complexity, fault analysis will rely solely on experimental data. However, collecting fault data without prior knowledge of the fault mechanism is costly and risky, especially for closed-loop systems.

Fault diagnostic usually can be seen as a three-step algorithm: 1) residual generator; 2) residual evaluator; 3) fault manager. The residual generator obtains residuals using extracted fault features. Then, the residual evaluator detects and locates faults by comparing the residual with prescribed thresholds. The fault manager takes control actions like alarming operators or triggering fault-tolerant controls. Recently, residual evaluators have been studied exclusively, especially employing machine learning and/or statistical techniques Wang et al. (2020); Sivaram and Sun (2023).

Due to its significance on diagnostic robustness, residual generation is the primary scope of this work. There are two technical categories for residual generation: 1) model-based approach; 2) signal processing-based approach. The former employs the residual based on state estimation or parameter estimation techniques, such as Lyapunov estimators Wu et al. (2012), Luenberger observers Khan et al. (2005); V. Mahulkar and Derriso (2011), Kalman filters Nurmi and Mattila (2012), and recursive parameter estimators Shi et al. (2005) to name a few. On the other hand, the latter employs the residual based on signal processing methods, including Fourier transform Yoon and Sun

^{*} Yongsoon Yoon (e-mail: yongsoonyoon@oakland.edu) is a corresponding author. This work was supported by the National Science Foundation under Grant CMMI-2301525.

(2022), empirical modal decomposition Goharrizi and Sepehri (2012) and wavelet Yazdanpanah Goharrizi and Sepehri (2010).

The authors have recently developed a novel closed-loop system diagnostic based on inverse model estimation and real-time monitoring of an inverse frequency response function (iFRF) Yoon (2023). To summarize briefly, firstly, the inverse model parameters are estimated by incorporating directional forgetting recursive least squares (DFRLS) Kulhavý and Kárný (1984) into an indirect two-stage closed-loop system identification scheme Van Den Hof and Schrama (1993). Secondly, the iFRF is computed using the estimated inverse model parameters and monitored in real-time for parametric fault diagnosis. The proposed diagnostic illustrates promising capabilities, especially in fault isolation, attributed to the iFRF, which reveals selective sensitivity to different parametric faults. However, the diagnostic performance turns out to be sensitive to input and output noises, which may adversely impact its robustness in practical applications.

In this work, the noise sensitivity of the previous method is addressed by incorporating adaptive Kalman filter (AKF) into an indirect two-stage inverse model estimation framework. The AKF features anti-windup capability, keeping eigenvalues of the covariance matrix bounded even in scenarios lacking sustained excitation, similar to DFRLS Gustafsson (2002): Medvedev (2003); Evestedt and Medvedev (2006). Additionally, it exhibits noise immunity, enabling robust inverse model estimation. Then, the iFRF, using the estimated inverse model parameters as a diagnostic residual, yields more comprehensive information for fault detection and isolation compared to conventional techniques, thereby enhancing the diagnostic robustness. Numerical validation showcases the enhanced robustness of the AKF-based inverse model estimation and subsequent iFRF analysis against variations in operational conditions and input/output noises, outperforming the previous approach based on DFRLS.

The remainder of the paper is outlined as follows: In Sec. 2, a physics-based inverse model is given together with brief sensitivity analysis. In Sec. 3, the proposed diagnostic is presented that encompassing two sequential steps. In Sec. 4, the effectiveness of the proposed method is numerically illustrated with application to an EHA. Finally, concluding remarks and future work are given in Sec. 5.

2. PHYSICAL MODEL

Figure 1 depicts a schematic of the linear EHA (cylinder-type) considered in this work. The voice coil motor (VCM) drives the spool-type directional control valve (DCV), which regulates the direction of the oil flow. In turn, this valve determines the resulting pressure differential across the piston, which ultimately drives the movement of the load.

A physics-based model of the EHA inherently exhibits nonlinear behaviors, attributed to factors such as nonlinear valve flow rate and friction. However, under appropriate assumptions, such as considering a linear valve flow rate while operating the EHA near equilibrium, and assuming a relatively high bandwidth of the directional control valve Yoon (2023), a continuous transfer function between the input (voice coil motor current), and output (load displacement) can be obtained as follows:

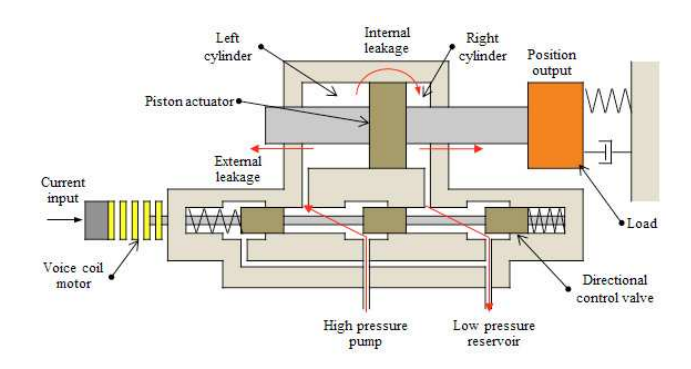


Fig. 1. A schematic of the linear electrohydraulic actuator.

$$G(s,\kappa) = \frac{A_p K_m C_d W \sqrt{\frac{P_s}{\rho}}}{\left(\frac{V_o}{2\beta} s + C_{ie}\right) \left(m_p s^2 + b_p s + k_p\right) + A_p^2 s}.$$
 (1)

Here, the transfer function depends on the Laplace variable: s and a diagnostic parameter vector $\kappa = [p_s, C_{ie}, b_p, \beta]^T$. Note that these parameters are carefully selected based on their practical significance on system diagnostic, as discussed in Eaton (1996); Wu et al. (2012); Yazdanpanah Goharrizi and Sepehri (2010). Please refer to Table 1 for the nomenclature of the model parameters used in (1).

Symbol	Description	Symbol	Description
m_p	Piston mass	β	Bulk modulus
b_p	Viscous coefficient	ρ	Oil density
k_p	Spring coefficient	C_d	Discharge coefficient
A_p	Cross-sectional area	Cie	Total leak coefficient
V_o	Cylinder volume	W	DCV area gradient
p_s	Supply pressure	K_m	VCM gain

Table 1. Nomenclature of model parameters

The inverse transfer function, which is the reciprocal of (1), is denoted as:

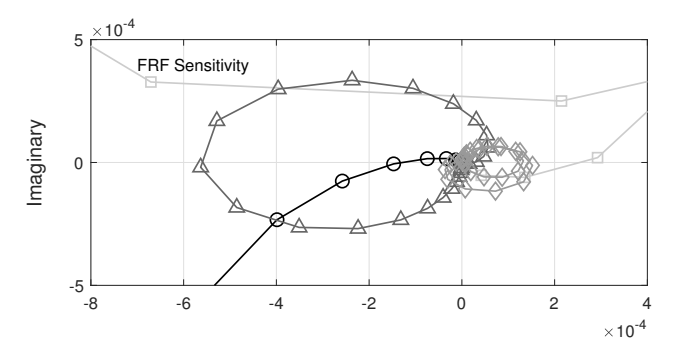
$$H(s,\kappa) = \frac{\left(\frac{V_o}{2\beta}s + C_{ie}\right)\left(m_p s^2 + b_p s + k_p\right) + A_p^2 s}{A_p K_m C_d W \sqrt{\frac{p_s}{\rho}}}.$$
 (2)

This inverse transfer function plays a crucial role in the proposed robust diagnostic Yoon (2023). Fig. 2 depicts the Nyquist plots of two fault sensitivities, defined as:

$$\tilde{\nabla}G(s, \kappa_o) = diag([p_{so} C_{ieo} b_o \beta_o]) \nabla G(s, \kappa)|_{\kappa_o}
\tilde{\nabla}H(s, \kappa_o) = diag([p_{so} C_{ieo} b_o \beta_o]) \nabla H(s, \kappa)|_{\kappa_o},$$

where $\nabla G(s, \kappa)|_{\kappa_o}$ and $\nabla H(s, \kappa)|_{\kappa_o}$ represent the Jacobian vectors of (1) and (2) with respect to the parameters at their nominal values, respectively. The Nyquist plots provide insights into the fault sensitivity of the inverse transfer function to different parameters. Notably, the inverse transfer function exhibits selective sensitivity to different parameters, which holds great potential for parametric fault diagnosis. It is worth noting that as frequency increases, the parametric fault selectivity becomes clearer due to the non-causality of the inverse transfer function.

The inverse transfer function of (2) is discretized using the Tustin method to formulate a recursive parameter estimation problem in Sec. 3. The input/output representation at discrete time k for the discrete time system is given by:



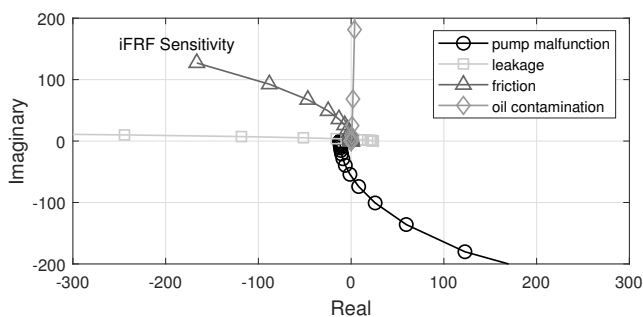


Fig. 2. Comparison of fault sensitivity functions, which are amplified gradient vectors with respect to the parameter vector: $\kappa = [p_s, C_{ie}, b_p, \beta]^T$. $\tilde{\nabla} G(s, \kappa_o)$ (upper) vs $\tilde{\nabla} H(s, \kappa_o)$ (lower)

$$u(k) = H(q^{-1}, \kappa)y(k)$$

$$= \frac{c_0(k) + c_1(k)q^{-1} + c_2(k)q^{-2} + c_3(k)q^{-3}}{1 + 3q^{-1} + 3q^{-2} + q^{-3}}y(k).$$
(3)

Here, q^{-1} represents the unit time delay operator, and $c_0(k)$, $c_1(k)$, $c_2(k)$, and $c_3(k)$ are the discrete time model parameters that depend on the physical model parameters given in Table 1 and sampling time Yoon (2023).

3. SYSTEM DIAGNOSTIC

Fig. 3 illustrates the overall structure of the proposed closed-loop system diagnostic. The upper part (I) represents the feed-back control responsible for operating the EHA as intended. The lower part (II) depicts the system diagnostic, which uses the closed-loop signals including the reference r(k), the control input u(k), and the controlled output y(k).

The system diagnostic itself consists of four main components: 1) inverse model estimator: this component is tasked with estimating the iFRF robustly using the closed-loop signals corrupted by input/output noises.; 2) residual generator: this component generates the residual based on the estimated iFRF.; 3) residual evaluator: this component detects and isolates parametric faults if present by classifying the residuals.; 4) fault alarm: this components triggers alarms and allows for fault-tolerant actions.

It is noted that the inverse model estimator and residual generator are the primary focus of this work, aiming to achieve robust estimation of the iFRF and effective fault detection and isolation capabilities despite the absence of persistent excitation and the presence of input/output noise.

3.1 Inverse Model Estimation using AKF

Based on (3), the input/output relationship can be written as:

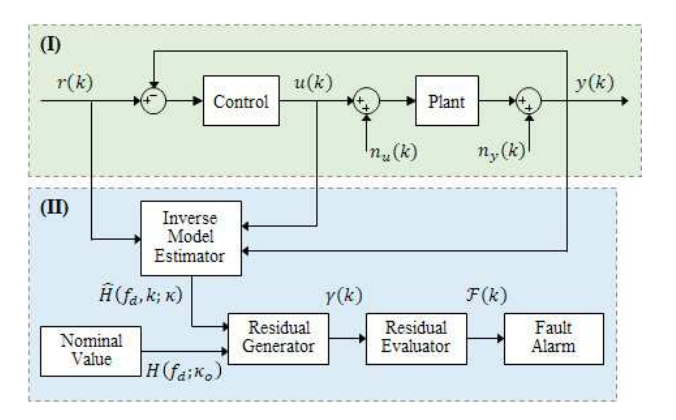


Fig. 3. The structure of the proposed closed-loop diagnostic

$$\eta(k) = \varphi^{T}(k)\theta(k), \tag{4}$$

where

$$\begin{split} & \eta(k) = u_a(k) + 3u_a(k-1) + 3u_a(k-2) + u_a(k-3) \\ & \varphi(k) = [y(k), \ y(k-1), \ y(k-2), \ y(k-3)]^T \\ & \theta(k) = [c_0(k), \ c_1(k), \ c_2(k), \ c_3(k)]^T \,, \end{split}$$

respectively. Note that in the closed-loop system depicted in Fig. 3, the closed-loop input is corrupted by input and output noises, denoted $n_u(k)$ and $n_y(k)$, respectively. To address this, a filtered and uncorrelated control input $u_a(k)$ is used for inverse model estimation instead of the raw control input u(k) within the indirect two-stage closed-loop system identification scheme Van Den Hof and Schrama (1993). Further details on the filtering process can be found in Yoon (2023).

The objective of the inverse model estimator is to estimate $\theta(k)$, which can vary due to the occurrence of parametric faults, using the available regressor vector $\varphi(k)$ and output $\eta(k)$. To apply the AKF, (4) is reformulated into a state-space model, assuming a random walk uncertainties d(k) and v(k) as follows:

$$\theta(k+1) = \theta(k) + d(k) \tag{5}$$

$$\eta(k) = \varphi^{T}(k)\theta(k) + v(k). \tag{6}$$

where d(k) and v(k) are the random walk uncertainties that are attributed to unknown parametric faults, and input/output noises, respectively. The covariances of these uncertainties are denoted by Q = Cov(d(k)) and R = Cov(v(k)).

Equations (7)-(10) below are the formula for the standard Kalman filter (KF).

$$\hat{\boldsymbol{\theta}}(k) = \hat{\boldsymbol{\theta}}(k-1) + K(k)e(k) \tag{7}$$

$$e(k) = \eta(k) - \varphi(k)^T \hat{\theta}(k-1)$$
(8)

$$K(k) = \frac{P(k-1)\varphi(k)}{R + \varphi(k)^T P(k-1)\varphi(k)}$$
(9)

$$P(k) = P(k-1) - \frac{P(k-1)\varphi(k)\varphi(k)^{T}P(k-1)}{R + \varphi(k)^{T}P(k)\varphi(k)} + Q, \quad (10)$$

where $\hat{\theta}(k)$ represents the parameter estimate, e(k) is the prediction error, K(k) is the Kalman gain, and P(k) is the covariance matrix. It is crucial to note that the effectiveness of the standard KF relies on the observability. If the system of (5) and (6) is observable, the standard KF ensures the optimal estimation of $\theta(k)$. However, in fact, observability is conditional, particularly if $\phi(k)$ undergoes persistent changes Gustafsson (2002). If it is not observable, the covariance matrix P(k) may increase unboundedly, leading to covariance windup, which can result in long and poor transient behaviors in estimation.

Differently from the standard KF using the constant covariance matrix Q in (10), the AKF employs the time-varying covariance matrix Q(k) that is adaptively updated based on the desired positive definite matrix P_d , the covariance of the output uncertainty v(k) denoted by R, and the output matrix $\varphi^T(k)$. Q(k) is updated using the following adaptation rule:

$$Q(k) = \frac{P_d \varphi(k) \varphi^T(k) P_d}{R + \varphi(k)^T P_d \varphi(k)}.$$
 (11)

The convergence property of the covariance matrix P(t) of the AKF is briefly reviewed based on Gustafsson (2002); Evestedt and Medvedev (2006). Let $e_p(k) = P(k) - P_d$ be the covariance matrix error. By applying matrix inversion lemma to $(P_d - Q(k))$ and (P(k+1) - Q(k)), the covariance matrix error at time k+1, denoted as $e_p(k+1)$, is given by:

$$e_p(k+1) = A_p(P(k))^{-1} e_p(k) A_p(P_d)^{-T},$$
 (12)

where $A_p(P(k)) = I + P(k)\varphi(k)R^{-1}\varphi(k)^T$. This implies that $e_p(k)$ converges to zero exponentially, which means that P(k) converges to P_d . Consequently, this achieves anti-windup capability regardless of the absence of persistent excitation. The balance between noise immunity and convergence rate can be adjusted by tuning the desired covariance matrix P_d .

3.2 Inverse Frequency Response Function Monitoring

Once $\hat{\theta}(k) = [\hat{c}_0(k), \hat{c}_1(k), \hat{c}_2(k), \hat{c}_3(k)]^T$ is available from (7), the time-varying iFRF can be computed as:

$$\hat{H}(f_d, k; \kappa) = \frac{\hat{c}_0(k) + \hat{c}_1(k)q^{-1} + \hat{c}_2(k)q^{-2} + \hat{c}_3(k)q^{-3}}{1 + 3q^{-1} + 3q^{-2} + q^{-3}}, \quad (13)$$

where $q^{-1} = \exp(j2\pi f_d/f_s)$, f_s is the sampling frequency, and f_d is the predetermined monitoring frequency in which the iFRF is analyzed. If any parametric fault occurs, i.e. the change in κ , it must be retained by $\hat{\theta}(k)$ and eventually by $\hat{H}(f_d, k; \kappa)$.

The diagnostic residual is defined as:

$$\gamma(k) = \hat{H}(f_d, k; \kappa) - H(f_d; \kappa_o), \tag{14}$$

where $H(f_d, \kappa_o)$ represents the known nominal iFRF at f_d . By monitoring the residual $\gamma(k)$ in real-time, one can diagnose whether a system has a fault (i.e. fault detection), and if so, what the fault source is (i.e. fault isolation). The diagnostic residual in (14) is a complex number, providing richer information compared to a real-valued residual. Additionally, the residual can be extended to a vector considering multiple frequencies such as:

$$\Gamma(k) = \begin{bmatrix} \gamma_1(k) \\ \vdots \\ \gamma_n(k) \end{bmatrix} = \begin{bmatrix} \hat{H}(f_{d_1}, k; \kappa) - H(f_{d_1}; \kappa_o) \\ \vdots \\ \hat{H}(f_{d_n}, k; \kappa) - H(f_{d_n}; \kappa_o) \end{bmatrix} \in \mathbb{C}^{n \times 1}$$

to generate more information for robust system diagnosis.

4. NUMERICAL VALIDATION

The nominal parameters in Yoon (2023) are used in numerical validation. The sampling frequency of the closed-loop system is $f_s = 100$ Hz. Random input/output noises are taken into account in the closed-loop simulation: $n_u \sim \mathcal{N}(0, 1e-8)$ and $n_y \sim \mathcal{N}(0, 1e-7)$. The PI controller is tuned to ensure closed-loop stability even in the presence of considered parametric faults. Fig. 4 shows the reference profile, which repeats every 10 seconds for 60 seconds, along with the resulting output

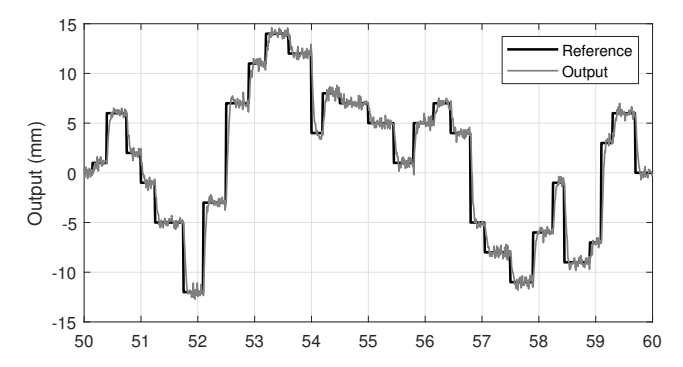


Fig. 4. Simulation conditions including transient and steady states: reference (dark gray) and controlled output (light gray).

signal using the nominal model parameters. As the simulation progresses, it gradually stabilizes, with the fitting degree of the signal in the last 10 seconds being the most reliable. Based on fault sensitivity analysis, parametric faults are injected with sizes as shown in Table 2. Note that only one fault is injected at a time.

Fault type	Parameter	Fault Size	
Pump malfunction	p_s	-40%, -20%, +20%, +40%	
Leakage	C_{ie}	+10%, +20%, +30%, +40%	
Friction	b_p	×10, ×20, ×30, ×40	
Oil contamination	β	×0.005, ×0.01, ×0.1, ×10	

Table 2. Sizes of the parametric faults injected.

Fig. 5 compares the estimated inverse model parameters with respect to the nominal model parameters using DFRLS (dark gray) and AKF (light gray). It is evident that the AKF offers a more robust estimation against input/output noise compared to DFRLS. The estimated iFRF with the pump malfunction (which is 40 % higher than the nominal) is shown in Fig. 6. The fault is injected at 30 seconds and persists since then. DFRLS and AKF demonstrate good fault-tracking capabilities despite a slight bias in the imaginary part, which has a relatively small impact compared to the real part. Fig. 6(b) illustrates how the iFRF evolves in the complex plane when the fault occurs. With both methods, the iFRFs converge quickly to the actual nominal values (indicated by the red star) until 30 seconds, and then to the abnormal values (indicated by the blue square) thereafter. This clearly demonstrates that the fault impact can be immediately captured by the iFRF for fault detection.

Fig. 7 shows the residuals in the complex plane during steady-state with different faults of varying sizes at different three diagnostic frequencies: $f_d = 1$ Hz (1st row), 10 Hz (2nd row), 20 Hz (3rd row). Note that in the nominal system, the residual should ultimately converge to the origin. In the first row, it is possible to differentiate between pump malfunction and leakage, but distinguishing between friction and oil contamination is challenging. Even with an increase of f_d to 10 Hz, a clear distinction remains elusive. However, as the frequency increases further to 20 Hz, the differentiation between friction and oil contamination becomes more pronounced. Distinct diagnostic residual patterns for each type and size of fault enable identification and isolation of specific faults, demonstrating the effectiveness of the proposed fault diagnosis method.

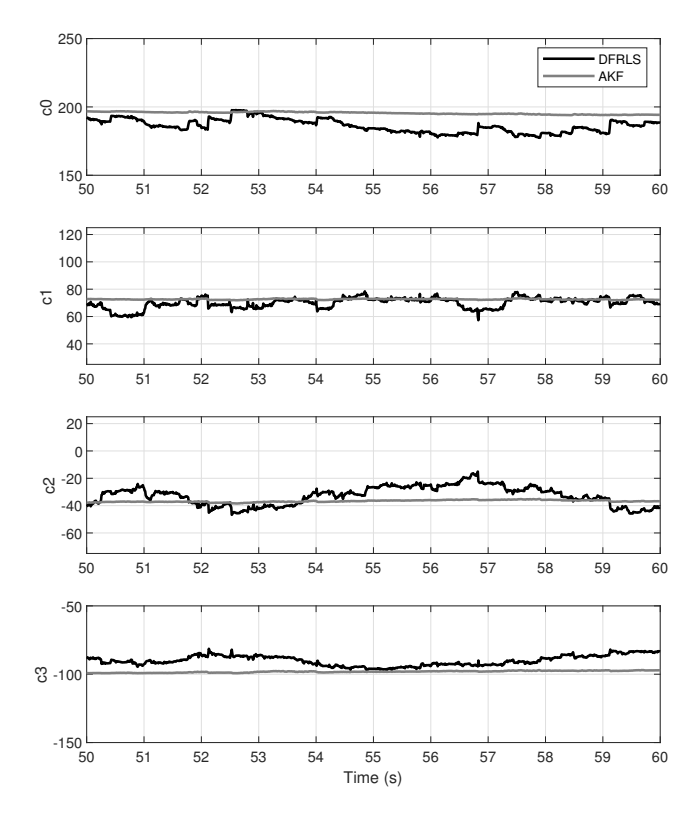


Fig. 5. Nominal parameter estimation of DFRLS (dark gray) and AKF (light gray)

To quantify the robustness of iFRF estimation and parameter estimation, the coefficient of variation (CV) are computed and compared. CVs are defined as:

$$\begin{split} CV_{\hat{\theta}} &= \sqrt{\frac{1}{4}\sum_{i=0}^{3}\frac{\sigma(\hat{c}_{i})}{\mu(\hat{c}_{i})}} \\ CV_{\hat{H}} &= \sqrt{\frac{1}{2}\left(\frac{\sigma(\text{Re}(\hat{H}))}{\mu(\text{Re}(\hat{H}))} + \frac{\sigma(\text{Im}(\hat{H}))}{\mu(\text{Im}(\hat{H}))}\right)} \end{split}$$

where σ and μ are the standard deviation and mean operator, and "Re" and "Im" indicate the real- and imaginary part of a complex number. The comparison of CVs is given in Fig. 8. The iFRF estimate shows much lower CVs, regardless of the estimation method, than the parameter estimate, which allows for more robust residual generation. It is noteworthy that AKF significantly reduces CV in both parameter estimate and iFRF compared to DFRLS.

5. CONCLUSION

This paper presents a fault diagnostic method for an EHA in closed-loop. The proposed diagnostic comprises two consecutive elements: Firstly, an AKF facilitates the robust estimation of inverse model parameters without encountering covariance windup, even amidst non-persistent excitation and noisy signals. Secondly, it involves the computation and monitoring of an iFRF, generating resilient residuals across multiple frequencies, thereby enhancing fault isolation capabilities. Numerical validation demonstrates the diagnostic robustness and rapid fault-tracking, enabling early and dependable fault diagnosis of EHAs. Further validation with multiple faults at a time will be done. Also, exploring nonlinear inverse models in the frequency domain to accurately capture fault impacts represents a promising avenue for future research.

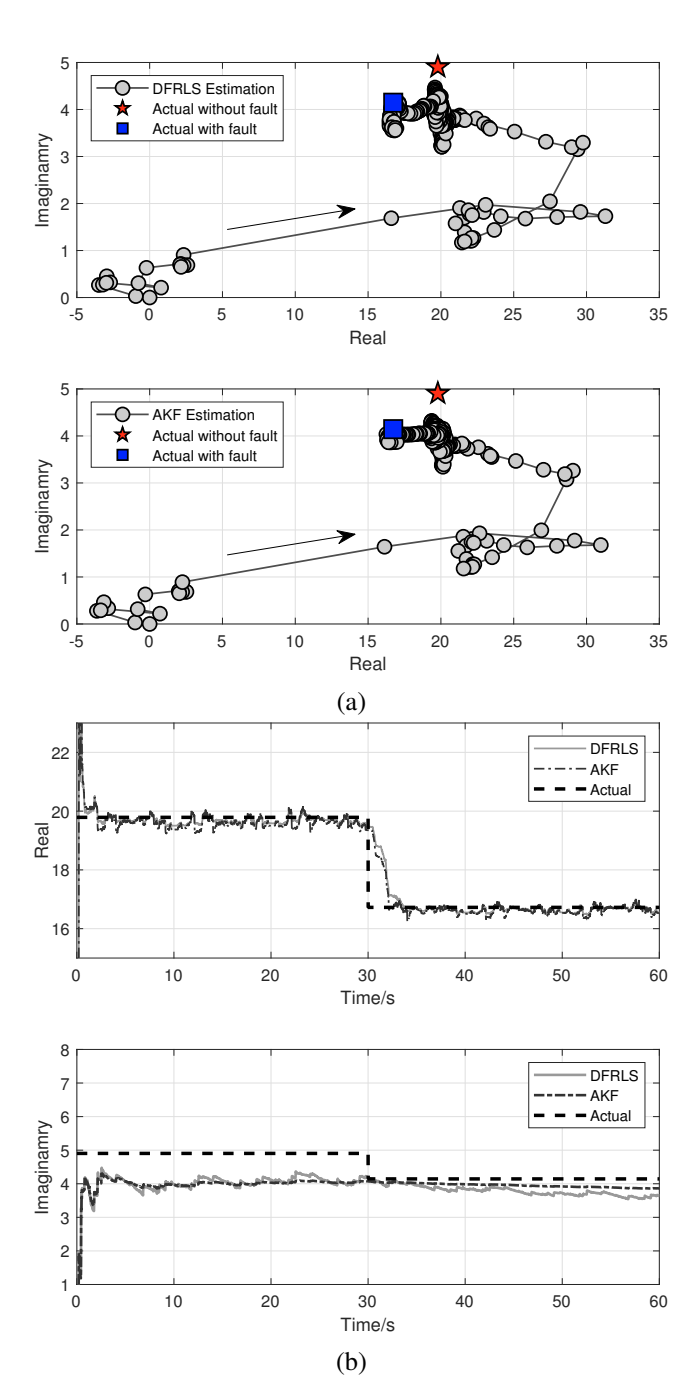


Fig. 6. iFRF traces at 1 Hz in complex domain (a), i.e. real vs imaginary, and in time domain (b), i.e. real vs time & imaginary vs time.

REFERENCES

Boaventura, T., Semini, C., Buchli, J., Frigerio, M., Focchi, M., and Caldwell, D.G. (2012). Dynamic torque control of a hydraulic quadruped robot. In *Proc. Int. Conf. Robotics Autom.*, 1889–1894. Saint Pual, MN, USA.

Chen, J. and Patton, R.J. (2012). Robust model-based fault diagnosis for dynamic systems, volume 3. Springer Science & Business Media.

Eaton (1996). Hydraulic hints & trouble shooting guide. General Product Support, Vicker.

Evestedt, M. and Medvedev, A. (2006). Stationary behavior of an anti-windup scheme for recursive parameter estimation under lack of excitation. *Autom.*, 42(1), 151–157.

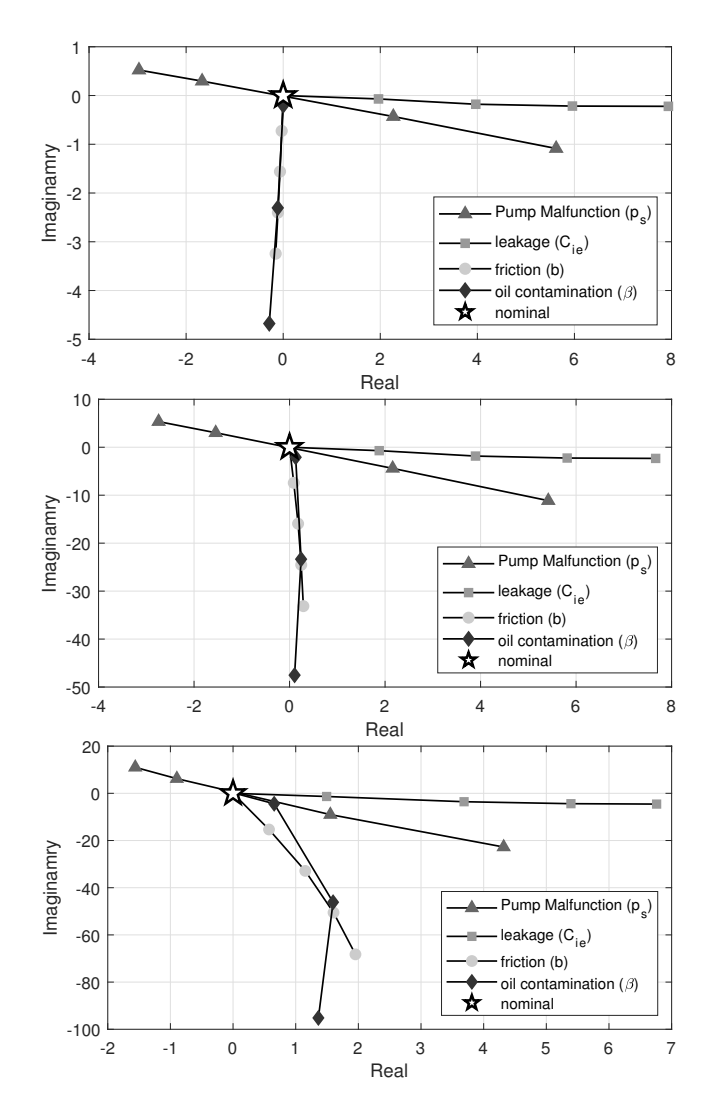


Fig. 7. Diagnostic residuals with different faults of varying sizes, as shown in Table 2, in the complex plane at 1 Hz (1st row), 10 Hz (2nd row), and 20 Hz (3rd row).

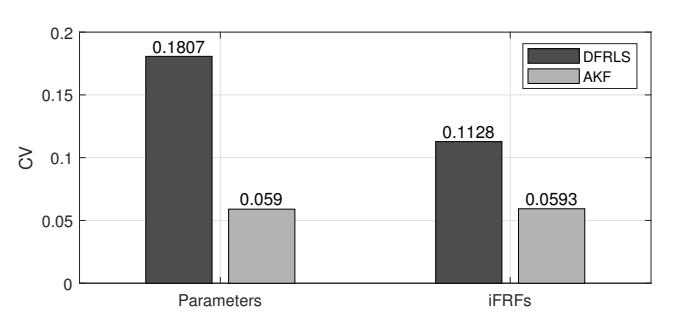


Fig. 8. Coefficient of variation (CV) of estimates: parameter vs iFRF and DFRLS vs AKF.

Forbes Technology Council Post (2022). Unplanned downtime costs more than you think. https://www.forbes.com/sites/forbestechcouncil/2022/02/22/unplanned-downtime-costs-more-than-you-think/?sh=79581e9536f7.

Frank, P.M. (1990). Fault diagnosis in dynamic systems using analytical and knowledge-based redundancy: A survey and some new results. *Autom.*, 26(3), 459–474.

Goharrizi, A.Y. and Sepehri, N. (2012). Internal leakage detection in hydraulic actuators using empirical mode decom-

position and Hilbert spectrum. *IEEE Trans. Instrum. Meas.*, 61(2), 368–378.

Gustafsson, F.K. (2002). Avoiding windup in recursive parameter estimation. In *Preprints of Reglermöte*, 148–153. Linköping, Sweden.

Karpenko, M. and Sepehri, N. (2009). Hardware-in-the-loop simulator for research on fault tolerant control of electrohydraulic actuators in a flight control application. *Mechatronics*, 19(7), 1067–1077.

Khan, H., Abou, S.C., and Sepehri, N. (2005). Nonlinear observer-based fault detection technique for electrohydraulic servo-positioning systems. *Mechatronics*, 15(9), 1037–1059.

Kulhavý, R. and Kárný, M. (1984). Tracking of slowly varying parameters by directional forgetting. In *Proceedings of the IFAC World Congress*, 687–692. Budapest, Hungary.

Medvedev, A. (2003). Stability of an windup prevention scheme in recursive parameter estimation. In *Proc. IEEE Conf. Decis. Control*, 399–404. Maui, HI, USA.

Nurmi, J. and Mattila, J. (2012). Detection and isolation of leakage and valve faults in hydraulic systems in varying loading conditions, part 2: Fault detection and isolation scheme. *Int. J. Fluid Power*, 13(1), 17–27.

Shi, Z., Gu, F., Lennox, B., and Ball, A. (2005). The development of an adaptive threshold for model-based fault detection of a nonlinear electro-hydraulic system. *Control Eng. Pract.*, 13(11), 1357–1367.

Sivaram, B. and Sun, Z. (2023). A fault diagnosis tool for electrohydraulic actuators. *ASME Letters Dyn. Syst. Control*, 3(2), 021001.

V. Mahulkar, D.E.A. and Derriso, M. (2011). Derivative free filtering in hydraulic systems for fault identification. *Control Eng. Pract.*, 19(7), 649–657.

Van Den Hof, P.M. and Schrama, R.J. (1993). An indirect method for transfer function estimation from closed loop data. *Autom.*, 29(6), 1523–1527.

Wang, J., Miao, J., Wang, J., Yang, F., Tsui, K.L., and Miao, Q. (2020). Fault diagnosis of electrohydraulic actuator based on multiple source signals: An experimental investigation. *Neurocomputing*, 417, 224–238.

Wu, X., Li, Y., Li, F., Yang, Z., and Teng, W. (2012). Adaptive estimation-based leakage detection for a wind turbine hydraulic pitching system. *IEEE/ASME Trans. Mechatron.*, 17(5), 907–914.

Yazdanpanah Goharrizi, A. and Sepehri, N. (2010). A wavelet-based approach to internal seal damage diagnosis in hydraulic actuators. *IEEE Trans. Ind. Electron.*, 57(5), 1755–1763.

Yoon, Y. (2023). Estimation and frequency domain analysis of an inverse model for electro-hydraulic system diagnostic in closed-loop. In *Proc. Am. Control Conf.*, 4703–4708. San Diego, CA, USA.

Yoon, Y. and Sun, Z. (2022). Recursive spectral analysis-based diagnostic with application to electrohydraulic actuators. *IEEE Control Syst. Lett.*, 6, 61–66.